Molecular diffusion in porous media by PGSE ESR

Yael Talmon,[a] Lazar Shtirberg,[a] Wolfgang Harneit,[b] Olga Yu. Rogozhnikova,[c] Victor Tormyshev[cd] and Aharon Blank*[a]

Received 21st October 2009, Accepted 9th March 2010
First published as an Advance Article on the web 6th April 2010
DOI: 10.1039/b922060g

Diffusion in porous media is a general subject that involves many fields of research, such as chemistry (*e.g.* porous catalytic pallets), biology (*e.g.* porous cellular organelles), and materials science (*e.g.* porous polymer matrixes for controlled-release and gas-storage materials). Pulsed-gradient spin-echo nuclear magnetic resonance (PGSE NMR) is a powerful technique that is often employed to characterize complex diffusion patterns inside porous media. Typically it measures the motion of at least $\sim 10^{15}$ molecules occurring in the milliseconds-to-seconds time scale, which can be used to characterize diffusion in porous media with features of $\sim$2–3 μm and above (in common aqueous environments). Electron Spin Resonance (ESR), which operates in the nanoseconds-to-microseconds time scale with much better spin sensitivity, can in principle be employed to measure complex diffusion patterns in porous media with much finer features (down to $\sim$10 nm). However, up to now, severe technical constraints precluded the adaptation of PGSE ESR to porous media research. In this work we demonstrate for the first time the use of PGSE ESR in the characterization of molecular restricted diffusion in common liquid solutions embedded in a model system for porous media made of sub-micron glass spheres. A unique ESR resonator, efficient gradient coils and fast gradient current drivers enable these measurements. This work can be further extended in the future to many applications that involve dynamical processes occurring in porous media with features in the deep sub-micron range down to true nanometric length scales.

1. Introduction

Many natural substances (such as rocks, soil, biological tissues, and bones) and man-made objects (*e.g.* cements, foams, storage containers, controlled-release matrixes, fuel cells, and catalytic pallets) are made of porous materials. The experimental observation and characterization of liquid transport processes in porous media are of significant value in a variety of scientific disciplines.[1,2] For example, civil engineers explore the transport of liquids through concrete and soil; environmental scientists observe processes of groundwater pollution in the ground by toxic liquids and hazardous wastes; chemists develop separation and catalytic methods based on porous substances; petroleum engineers examine oil transport in porous rock formations; medical researchers investigate processes in porous tissues such as the kidneys and lungs; and biologists are interested in metabolite and protein transport in porous cellular organelles such as centrosomes.

Over the last four decades, liquid-state nuclear magnetic resonance (NMR) *via* the pulsed-gradient spin-echo (PGSE) technique and its variants has been employed to measure restricted and anisotropic diffusion in various types of porous media.[3–8] The wide availability of NMR systems and the possibility of combining diffusion measurements with imaging[9] has made this technique very popular and it is considered to be one of the most accurate and versatile methods of diffusion measurement.[10]

Despite the great success of PGSE NMR and related techniques, they are still known to suffer from some fundamental physical limitations that are attributed to all NMR-based techniques. Thus, for example, the limited sensitivity and the relatively long time scales of the processes in liquid-state NMR directly affect PGSE NMR capabilities. Typically, it measures collective motions of at least $\sim 10^{15}$ molecules or more occurring in the milliseconds-to-seconds time scale. For *aqueous-like viscosity* (typically $D \approx 10^{-9}$ m^2 s^{-1}) this time scale corresponds to motions over distances that cannot be smaller than $\sim$2–3 μm.[11] Furthermore, when diffusion measurement is combined with spatial imaging, some limitations arise with respect to the limited image resolution of MRI (commonly not better than $\sim$20–30 microns) and the relatively long image acquisition time (cannot be shorter than $\sim$100 ms, even with the most advanced systems).[12]

Recently, we have shown for the first time that PGSE can also be employed in conjunction with liquid-phase ESR to directly measure the diffusion coefficient of paramagnetic species in *homogenous* solutions.[13] PGSE ESR typically operates in the microseconds time scale and thus can be complementary to the NMR-based approaches. Furthermore, the greater sensitivity (up to $\sim 10^7$ molecules) and specificity (using stable

[a] *Schulich Faculty of Chemistry, Technion—Israel Institute of Technology, Haifa 32000, Israel. E-mail: ab359@tx.technion.ac.il; Fax: +972-4-829-5948; Tel: +972-4-829-3679*
[b] *Institut für Experimentalphysik, Freie Universität Berlin, Arnimallee 14, 14195 Berlin, Germany*
[c] *Novosibirsk Institute of Organic Chemistry, 9, Academician Lavrentyev Avenue, 630090 Novosibirsk, Russia*
[d] *Novosibirsk State University, 2 Pirogov Street, 630090 Novosibirsk, Russia*

free radicals or spin labels—similar to fluorescent labels in optics) of the ESR technique at ambient conditions can be of importance in many biological and materials science applications. (Although, as shall be shown below, further improvements must be made before PGSE ESR can be employed with some of the more common, biologically relevant, nitroxide radical spin labels.) It should be noted that many other methods can be used for the measurement of translational motion in various time and distance scales; for example, neutron scattering,[14] optical fluorescence photobleaching,[15] fluorescence correlation spectroscopy,[16] and single molecule tracking.[17] However, these methodologies are complementary to both the NMR- and mainly the ESR-based methods (see Fig. 1 in ref. 13), since they operate at different time and distance scales, far from the ~μs per 100 nm which are the typical time/length scales of PGSE ESR.

The present work continues our recent efforts and shows that PGSE ESR can indeed be expanded to investigate and characterize the restricted diffusion of common liquid solutions in porous media with features in the sub-micron length scale that occurs during the 10–100 μs time scale. These capabilities were realized by the use of a miniature pulsed ESR resonator, tiny efficient gradient coils, and powerful fast gradient drivers, which greatly improve upon our previous work and facilitate better spin sensitivity and stronger and faster gradient pulses.

2. Theory and experimental challenges

As noted before,[13] the short time scale of the ESR experiment poses significant technical difficulties to the experimentalist who wishes to investigate diffusion with ESR, more so if one is interested in looking at restricted diffusion in porous media. The equation that describes the measured echo signal in a typical stimulated echo PGSE experiment (Fig. 1[18]), for the case of unrestricted diffusion, is as follows:[3]

$$E_{(t=2\tau_2+\tau_1)} = A\exp\left(-R - D\gamma^2\left(\int_t^{t+\delta} g(t)\mathrm{d}t\right)^2(\Delta-\delta/3)\right) \quad (1)$$

where A describes the maximum amplitude of the echo, $R = 2\tau_2/T_2 + \tau_1/T_1$, T_1 and T_2 are the spin–lattice and spin–spin relaxation times of the measured spin, respectively, D is the diffusion constant, γ is the gyromagnetic ratio, and

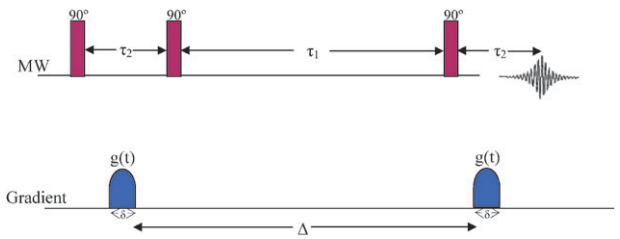

Fig. 1 Pulse sequence for stimulated echo pulsed gradient employed in the present work. The half-sine-shaped pulsed field gradients have varying amplitude ($g(t)$) and a typical duration of δ. A 16-step phase cycling scheme was used to cancel all unwanted FID and echo signals.[18]

τ_1, τ_2, Δ, δ, and g are the pulse-related parameters defined in Fig. 1. In order to properly quantify the value of D, the relation $D\gamma^2\left(\int_t^{t+\delta} g(t)\mathrm{d}t\right)^2(\Delta-\delta/3) \geq R$ must be approached (otherwise, the effect of the diffusion on the echo signal would be too small compared with the relaxation effects). If we assume that the time scale of the experiment is comparable to T_1 and T_2 (*i.e.* $R \approx 1$), then one must meet the condition of $D\gamma^2\left(\int_t^{t+\delta} g(t)\mathrm{d}t\right)^2(\Delta-\delta/3) \geq 1$. In ESR the time scale is ~3 orders of magnitude shorter than in NMR, while γ is ~3 orders of magnitude larger. However the term $D\gamma^2\left(\int_t^{t+\delta} g(t)\mathrm{d}t\right)^2(\Delta-\delta/3)$ has a cubic dependency in the time scale and only a quadratic dependence in γ, which means that in order to have the same influence by diffusion, the gradient in ESR must be $\sim\sqrt{1000}$ or ~1.5 orders of magnitude stronger than that in common PGSE NMR experiments (in addition to being much shorter). As we recently described, new ESR probes and a fast/strong gradient driver methodology enabled us to produce short (~1 μs) gradients of ~50 T m^{-1}. These gradients, together with the high signal-to-noise ratio (SNR) obtained for small samples with our miniature resonator, make it possible to meet the required conditions for measuring unrestricted diffusion in common solvents.[13]

Further to this work, in order to properly address the challenges of measuring and characterizing restricted diffusion processes in porous media, one has to increase the gradient strength and improve the SNR of the system. If we consider, for example, the pioneering work of Callaghan and co-workers, looking at diffusion of water in a matrix of glass microspheres, the echo amplitude due to diffusion processes is given by:[5]

$$E_\Delta(q) = |S_0(q)|^2 \times \exp\left(-\frac{6D_{\mathrm{eff}}\Delta}{b^2+3\xi^2}\left(1-\frac{\sin(2\pi qb)}{2\pi qb}\mathrm{e}^{-2\pi^2q^2\xi^2}\right)\right) \quad (2)$$

where

$$S_0(q) = \frac{3(2\pi qa\times\cos(2\pi qa)-\sin(2\pi qa))}{(2\pi qa)^3} \quad (3)$$

and

$$q = \frac{\gamma\int_t^{t+\delta} g(t)\mathrm{d}t}{2\pi} \quad (4)$$

The factor $S_0(q)$ is the q-space Fourier transform of the spin density in a single pore (unit cell) in the porous media, which in this case is approximated to a sphere with radius a. The parameter D_{eff} is the self-diffusion coefficient of the Brownian motion for long-range migration between the pores, b is the mean spacing between the pores, and ξ is the standard deviation of b. In order to adequately examine such type of porous medium and characterize the size of its pores, the distance between the pores, and the diffusion inside the pores and from pore to pore, several conditions must be met at the same time. First, in order to observe motions from pore to pore, the diffusion time, Δ, should be $\Delta \approx b^2/2D_{\mathrm{eff}}$. In addition, the magnitude of q should be $q \approx 1/b$, so that the echo signal as a function of q exhibits a "diffraction pattern" characteristic of the periodicity of b.[5,9] Furthermore, free diffusion inside the pores can be observed only if the diffusion time obeys the condition $\Delta < a^2/6D$; while for longer diffusion times, a

diffraction pattern of the individual pores would appear only by using high gradients that maintain $q \approx 1/a$.

The conditions presented in the last paragraph can be used to demonstrate the notion that PGSE NMR and ESR are complementary approaches. For example, in the case of PGSE NMR, for a diffusion coefficient typically encountered in aqueous solutions (in the range of $D \approx 10^{-9}$ m^2 s^{-1}) and for the typical range of Δ ($\sim$10–1000 ms), one can expect to characterize the porous media described above with a and b values in the range of $\sqrt{6D\Delta_{min}} \approx 8$ to $\sqrt{2D\Delta_{max}} \approx 50$ microns. This characterization would require q values of up to $1/a \approx 125\,000$, which, for a typical NMR gradient pulse duration of 1 ms, imply peak gradient values of $\sim$3 T m^{-1}. On the other hand, for PGSE ESR the typical values for the diffusion time are $\Delta \approx$ 1–100 μs (see ref. 13 and the work presented below). Using the above-stated arguments, one can find that the relevant a and b values for observation in aqueous conditions are in the range of $\sim$80 to $\sim$500 nm. The required q values are therefore between 2×10^6 to 12.5×10^6 for useful observation of porous media with such features (the smaller q is sufficient for $\sim$500 nm and the larger q is required for $\sim$80 nm). These values of q, for typical gradient pulse durations of 1 μs, imply peak gradient values of $\sim$75 T m^{-1} up to $\sim$460 T m^{-1}.

It should be noted that under conditions of very slow diffusion ($<10^{-11}$–10^{-13} m^2 s^{-1}), NMR with very strong ($\sim$50–100 T m^{-1}) but long or even constant gradients can be used to characterize features in porous media down to the $\sim$10 nm length scale, but still with the limitation of looking at processes occurring in the $\sim$ms time scale and above.[19,20] Furthermore, one should also note that in the unique case of ESR using conduction electrons in the solid phase, one can encounter diffusion coefficients in the range of $\sim 10^{-4}$ m^2 s^{-1}, which enable observing both restricted and unrestricted diffusion effects with PGSE ESR in relatively large pores ($\sim$200 μm) without the need for very powerful gradients (*i.e.* only $\sim$0.4 T m^{-1}).[21,22]

It is therefore evident that ESR offers the possibility of exploring the characteristics of diffusion in porous media under aqueous environment in length *and* time scales that are well beyond the reach of PGSE NMR (and also beyond the reach of other methods; see Fig. 1 in ref. 13). The "price" that has to be paid for such a capability is that new methodological tools must be developed to facilitate very strong gradients, well beyond what is available in NMR, over relatively short time scales. Furthermore, since the diffusion measurements also require monitoring signal decay, often over 1–3 decades, sufficient SNR is needed to obtain $E(q)$ graphs of good quality that can be fitted to the theoretical curves and enable proper parameter extraction.

3. Experimental details

3.1 Materials preparation

$N@C_{60}$ was synthesized by continuous nitrogen ion implantation into freshly sublimed fullerene layers with a yield ($N@C_{60}$: C_{60} ratio) of $\sim$0.01% as described elsewhere.[23] The $N@C_{60}$ contained in the harvested product was enriched and purified by multi-step high-pressure liquid chromatography (HPLC).[24] Sample purity was checked by UV-Vis absorption and analytical HPLC. The fullerene content of the sample is estimated to be better than 99.5%, consisting mostly of diamagnetic species C_{60} (83.7%), its epoxide $C_{60}O$ (14.4%), and trace amounts ($<$0.3%) of C_{70}. The $N@C_{60}/C_{60}$ ratio of 1.6(3)% was quantified using analytical HLPC and electron spin resonance as described earlier.[25]

"Finland D36" trityl (tris-(8-carboxyl-2,2,6,6-tetrakis-(D_3-methyl)-benzo[1,2-*d*:4,5-*d*′]bis(1,3)dithiol)methyl sodium salt) was synthesized using the method shown in Fig. 2, which is described in detail below.

Tris-(2,2,6,6-tetrakis(D_3-methyl)-benzo[1,2-*d*:4,5-*d*′]bis(1,3)-dithiol)methanol (I). Compound **I** was prepared by analogy with a known literature multi-step procedure.[26] Compound **I** and all the additional diamagnetic intermediates possessed, within the error limits of ^{1}H NMR integration, the same percentage of deuterium of 89.4 ± 0.6% for methyl groups of acetonide fragments.

Tris-(8-ethoxycarbonyl-2,2,6,6-tetrakis(D_3-methyl)-benzo[1,2-*d*:4,5-*d*′]bis(1,3)dithiol)methanol (II). A 1.9 M pentane solution of *tert*-BuLi (2.89 mL, 5.5 mmol) was added dropwise over 10 min to a stirred suspension of **I** (0.460 g, 0.5 mmol) and freshly distilled TMEDA (0.696 g, 6 mmol) in *n*-hexane

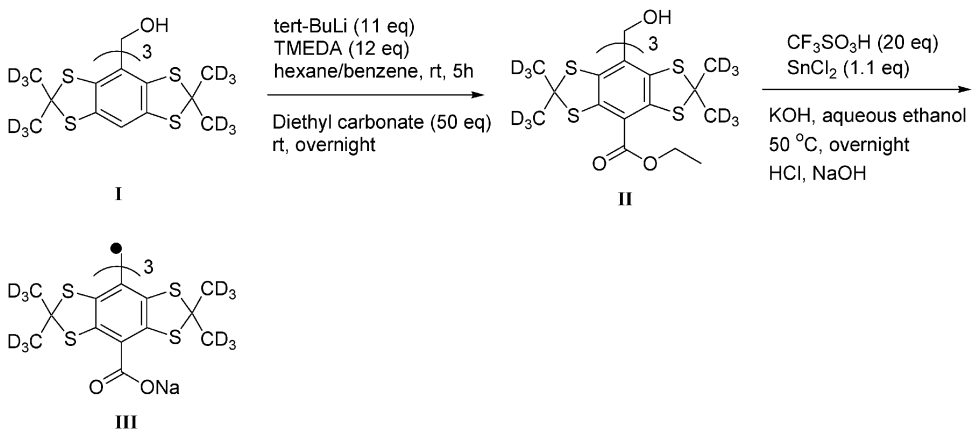

Fig. 2 Synthesis scheme of the "Finland D36" trityl.

(2 mL) at 0 °C (bath temperature). After the mixture was stirred at room temperature (RT) for 3.5 h, benzene (1.5 mL) was added. The resulting greyish-brown solution was stirred at RT for an additional 1.5 h and then added to diethyl carbonate (2.95 g, 25 mmol) cooled at −15 °C bath temperature. The cold bath was removed and stirring was continued at RT overnight. Saturated aqueous NaH_2PO_4 (2 mL) and ether (10 mL) were added. The organic phase was separated, filtered through a short plug of silica and concentrated *in vacuo*. The crude product (red syrup) was purified by column chromatography on a silica gel (dichloromethane–hexane, from 1 : 4 to 1 : 1), followed by re-crystallization from acetonitrile (7 mL) to generate the title product **II** (0.204 g, 36%) as a lemon-yellow powder: mp > 270 °C (gradually decomposed); ^{1}H NMR (300 MHz, $CDCl_3$): δ = 1.43 (t, 9H, J = 7.1 Hz, CH_3CH_2O), 4.41 (m, 6H, CH_3CH_2O), 6.75 (s, 1H, O*H*); ^{13}C NMR (75.47 MHz, $CDCl_3$): δ = 14.41 (q), 28.80 (q), 29.36 (q), 32.01 (q), 33.98 (q), 61.01, 61.09, 62.48, 84.46 (s), 121.46 (s), 134.14 (s), 139.40 (s), 140.50 (s), 141.60 (s), 142.00 (s), 166.34 (s); HPLC purity > 97%.

Tris-(8-carboxyl-2,2,6,6-tetrakis(D_3-methyl)-benzo[1,2-*d*:4,5-*d*′]-bis(1,3)dithiol)methyl sodium salt (III). A solution of CF_3SO_3H (0.339 g, 2.26 mmol) in dry acetonitrile (0.5 mL) was added dropwise over 10 min under argon to a stirred solution of **II** (0.125 g, 0.113 mmol) in dichloromethane (4.5 mL). After the mixture was stirred at RT for 10 min, a solution of $SnCl_2$ (0.0245 g, 0.124 mmol) in dry THF (1.5 mL) was added. The resulting dark brownish-green solution was stirred at RT for 15 min, after which it was quenched with saturated aqueous NaH_2PO_4 (5 mL). The mixture was diluted with chloroform (5 mL) and stirred vigorously for 2 min. The organic layer (lower one) was separated, washed with brine, dried ($MgSO_4$), filtered, and concentrated *in vacuo* to produce the crude triester trityl as a black solid. Ethanol (1.5 mL), dioxane (1 mL) and a solution of KOH (0.063 g, 1.13 mmol) in water (0.25 mL) were added. The mixture was stirred at 50 °C under argon for 2 h, after which all solvents were removed *in vacuo*. Water (4 mL) was added. After being stirred overnight under argon at RT, the resulting deep-green solution was passed through a paper filter and acidified with 2 M HCl to pH 2. The precipitated triacid was extracted with ether (3 × 10 mL). The combined organic extract was dried ($MgSO_4$), filtered, and concentrated *in vacuo* to produce the crude triacid trityl as a black solid (0.109 g, 0.105 mmol). MALDI-TOF: calculated for $[C_{40}H_3D_{36}O_6S_{12} + H]^+$ 1036.17; found 1036.41.

The triacid was dissolved in 0.1 M aqueous NaOH (3.16 mL, 0.316 mmol). The solution was left standing at RT for 10 min, filtered, and concentrated *in vacuo* to generate the title product (0.113 g, 93%) as a greenish-black powder. HPLC purity >97%. ESR (Bruker EMX CW at X-band, 0.3 mM deoxygenated water solution): line width 32 mG.

3.2 Sample preparation

The enriched N@C_{60} sample was dissolved in carbon disulfide (99.9%—from Spectrum Chemicals), which resulted in a room-temperature saturated solution concentration of ~0.15 mM (for the N@C_{60}). In parallel, a water suspension of 0.51 micron diameter glass spheres (from Bangs Laboratories, US) was placed inside a capillary glass tube with an inner diameter of ~0.5 mm. The tube was then placed in an ultracentrifuge and spun at 4000 rpm in order to pack the spheres at its bottom. The remaining water in the tube was removed in vacuum while the tube was subjected to heat at ~100 °C. The solution of N@C_{60} in the CS_2 was then inserted into the capillary tube, which was sealed using a flame torch. The tube was left for a week at ambient conditions prior to the measurements to enable sufficient time for the solution to diffuse into the matrix of dry glass spheres. Additional tubes without the glass spheres containing N@C_{60} in CS_2 and N@C_{60} in 1-chloronaphthalene were prepared for reference measurements of unrestricted diffusion. The trityl samples were prepared by adding 1 mM trityl water solution to the above-described capillary tubes with glass spheres in diameters of 0.32 and 0.51 microns. These samples were sealed under vacuum after oxygen was removed using several freeze–pump–thaw cycles. An additional tube without the glass spheres (containing just the trityl water solution) was prepared for reference measurements of unrestricted diffusion.

The relaxation times of the N@C_{60} and trityl solutions were measured recently,[13] with the following results: for N@C_{60} in 1-chloronaphthalene, T_1 and T_2 were found to be 33.3 and 6.4 μs, respectively. For N@C_{60} in CS_2 the measured values are 91 and 14.3 μs, and for the trityl in water 16.7 and 5 μs, for T_1 and T_2, respectively.

3.3 Experimental setup

The PGSE ESR experiments were carried out with our "home-built" pulsed ESR imaging system (described before in ref. 13,27). In the present work we have employed a new probe that was specifically designed and constructed to support such type of diffusion measurements by ESR (shown in Fig. 3). In addition to the new probe, the ESR system underwent some software and microwave hardware improvements that provided better signal sensitivity and stability compared with our recent work.[13]

The new probe operates at ~15.5 GHz and is comprised of a double-stacked dielectric ring resonator made of a high-permittivity (ε = 300) single crystal of $SrTiO_3$. The inner diameter of each ring is 0.76 mm and the outer diameter is 1.4 mm. The height of each ring, as well as the gap between the two rings, measures 0.3 mm, resulting in an overall resonator height of 0.9 mm, which is optimized for accommodating samples in capillary tubes. The resonator is located inside a cylindrical glass tube (id 2.6 mm, od 3 mm) with a 1 μm gold shield deposited on its exterior (by evaporation in a vacuum chamber). This shield acts as a barrier that prevents the microwave from escaping out of the resonator but still allows the low frequency field generated by the gradient coils to penetrate inside. This enables maintaining a high quality factor for the microwave resonator, while avoiding eddy currents due to the fast pulsed gradients. Small and efficient gradient coils are positioned on the glass cylindrical shield.

This diffusion probe is equipped with X- and Z-gradient coils as well as static-field bias coils to enable field frequency lock (FFL) capability. The structure of the X-gradient coil is based on a simple Maxwell pair with a high degree of

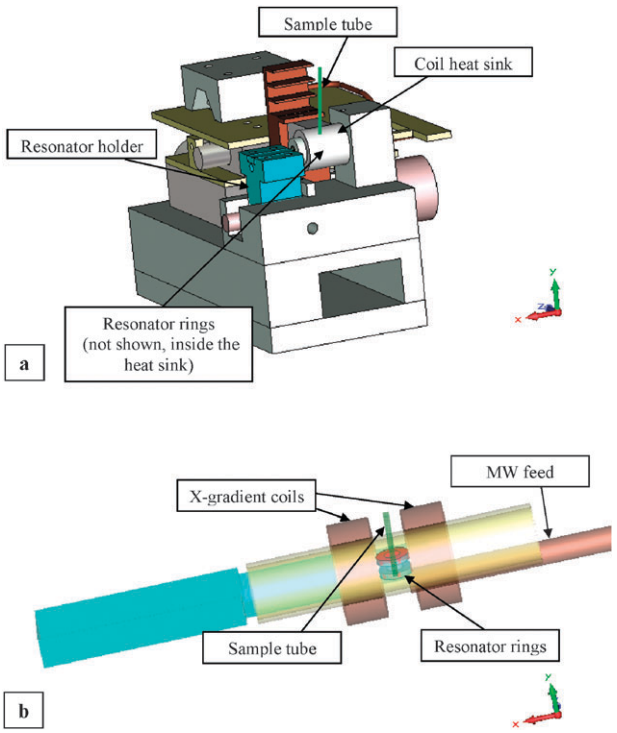

Fig. 3 (a) General overview of the PGSE ESR probe. (b) Close view of the resonator inside the probe, with the heat sink section removed from the figure. The Z-gradient coils and static-field bias coils are also not shown here.

efficiency. The coils of the pair are connected in parallel and have a total inductance of 1.0 μH, a resistance of 0.5 Ohm, and produce a magnetic gradient of 2.43 T m^{-1} A. A Z-gradient coil is positioned on top of the X-gradient coil. It is based on Golay geometry but with a serial connection between the upper and lower parts of the coil and has an efficiency of 1.31 T m^{-1} A. Its total inductance is 8.9 μH and its resistance is 1.8 Ohm. This coil can be used in constant-current mode to reduce field homogeneity near the sample and therefore to improve the cancellation of the free induction decay (FID) signal that may interfere with the relatively low-amplitude stimulated echo signal. (However, it was not necessary to use it in the experiments presented here.) The efficiency of the gradient coils was calculated by "home-made" Matlab software based on the Biot–Savart law. The calculations were verified experimentally (for the X-gradient coil) by applying a constant (DC) 0.1 A current directly into the gradient coils and measuring the broadening of the N@C_{60} sample ESR signal in the frequency domain. Knowing the size of the sample, one can directly calculate from the signal broadening the gradient strength for 1 A of drive current (as provided above).

4. Results

4.1 Unrestricted diffusion in reference samples

The initial step in the present set of experiments was to repeat part of our previous work—measuring unrestricted diffusion[13]—with the use of the new probe and the improved ESR system. This enabled us to evaluate the performance of the new probe and ESR system which, as shall be shown below, indeed provide a much better quality of results with enhanced stability and higher SNR. The first thing we tested was the level of "signal reconstruction", with several sets of τ_1 and τ_2 in the pulse sequence, and with a variety of gradient strengths. The term "signal reconstruction" can be explained as follows: ideally, when the diffusion effect is negligible, the same echo signal magnitude should be measured with and without the gradients (*i.e.* complete "signal reconstruction"). In our previous work, gradient pulses of ~50 T m^{-1} applied for ~900 ns resulted in a relatively poor signal-reconstruction level of only ~15%. This was mainly due to residual currents in the gradient coils that still linger on during the echo acquisition and distort its signal (eddy-current effects are negligible in the dielectric resonator we employ). The new probe enabled much better "signal reconstruction" levels of ~35–40% with a much stronger gradient pulse of ~100 T m^{-1}, applied for ~1200 ns (for typical τ_1 = 20 μs and τ_2 = 2.5 μs). The level of "signal reconstruction" was measured using a sample of N@C_{60} in 1-chloronaphthalene, which has relatively high viscosity and therefore should exhibit a minimal echo-signal reduction effect due to diffusion. This was carried out by recording the reduction in the stimulated echo signal as a function of the increasing gradient magnitude for fixed τ_1 and τ_2 values. We assumed a diffusion coefficient for the N@C_{60} in 1-chloronaphthalene based on the Stokes–Einstein expression (see below). The theoretical diffusion coefficient enabled us to estimate the theoretically-expected signal reduction due to diffusion alone (eqn (1)), which is relatively small for this type of sample, leading to the conclusion that the additional signal decay is due only to the effect of the residual transient magnetic fields.

Following this preliminary stage of work, unrestricted diffusion in homogenous solution was measured using the three types of samples described above (N@C_{60} in 1-chloronaphthalene, N@C_{60} in CS_2, and trityl in water). Two types of measurements were preformed. In the first type, the echo signal was recorded using the sequence shown in Fig. 1 for different τ_1 values while τ_2 remained constant. Gradient intensity (g) and gradient duration (δ) were also kept constant. The results of this measurement are summarized in Fig. 4a, which shows the natural logarithm (ln) of the echo signal ratio $(\ln(s/s_0)$ as a function of the factor $\tilde{q} = \gamma^2\left(\int_t^{t+\delta} g(t)\mathrm{d}t\right)^2 \Delta$. For trityl in water, the gradient intensity was set to 100 Tesla m^{-1}, and τ_1 was varied from 10 μs to 60 μs in 10 μs steps. For N@C_{60} in 1-chloronaphthalene the gradient intensity was set to 92 Tesla m^{-1} and τ_1 was varied from 20 μs to 60 μs in 5 μs steps. For N@C_{60} in CS_2 the gradient intensity was set to 62 Tesla m^{-1} and τ_1 was varied from 10 μs to 40 μs in 5 μs steps. The lower time threshold of 10 μs was limited by our gradient drivers' system. The upper time threshold is limited by the T_1 of the tested sample while taking under consideration the available SNR and the extent of the signal attenuation due to diffusion. For all samples δ was set to 1.2 μs and τ_2 was 2.5 μs. Every recorded echo subjected to the pulsed field gradients (with signal magnitude denoted as s) was followed immediately by the recording of an echo signal without gradients (denoted as s_0). The ratio between the two signals

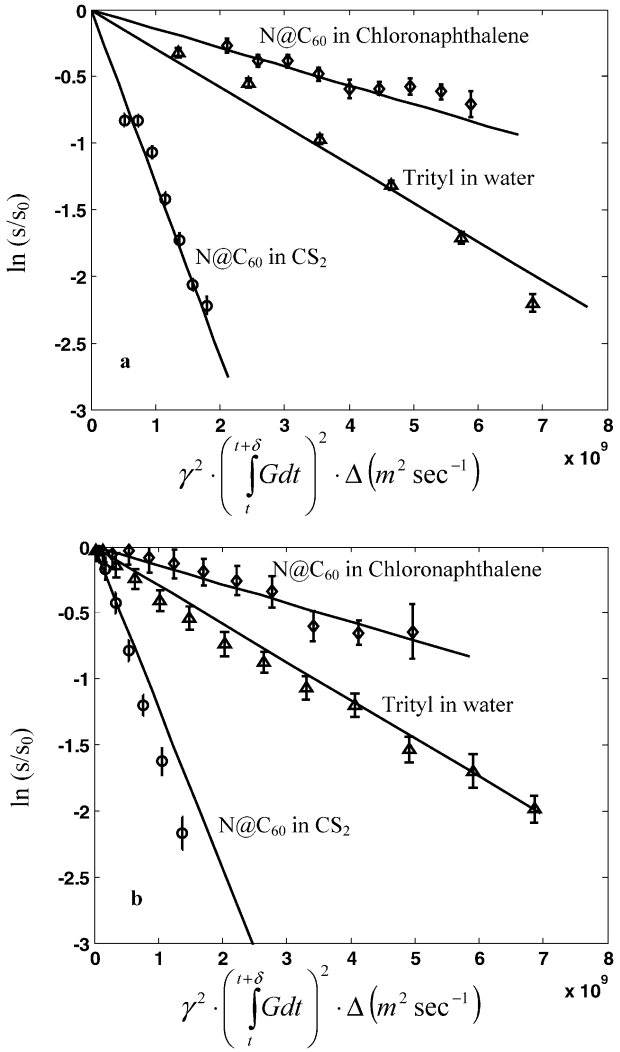

Fig. 4 (a) Stejskal–Tanner plot of the stimulated echo's ln magnitude as a function of the factor $\tilde{q} = \gamma^2\left(\int_t^{t+\delta} g(t)\mathrm{d}t\right)^2 \Delta$ for $N@C_{60}$ in 1-chloronaphthalene (◊) and in CS_2 (Δ) and for trityl in water (○). The straight lines are fitted curves for the slope that corresponds to the experimental D values (based on eqn (1)). The values of $\tilde{q}$ were varied by changing τ_1 in the pulse sequence, while keeping all other parameters of the pulse sequence constant. $\tilde{q}$ was calculated based on the measured integral of the half-sine gradient pulse. (b) Plot similar to (a) but in this experiment the values of $\tilde{q}$ were varied by changing the amplitude of the peak g value while keeping all other parameters of the pulse sequence constant.

(s/s_0) eliminates the relaxation effects and represents only the diffusion-related signal decay (see eqn (1)), as well as the effect of the residual transient magnetic fields of the gradient pulse at the time of the echo (*i.e.* the limited capability to achieve full "signal reconstruction" as described above). Since the gradient value and τ_2 are constant in this type of experiment, the effect of the residual transient magnetic fields on the s/s_0 ratio is the same for all the τ_1 values and does not affect the slope of the graph in Fig. 4a. Therefore, the diffusion coefficient can be extracted directly from the slope of this graph, based on eqn (1).

The second type of experiment is conducted using the same pulse sequence (Fig. 1) but applying constant τ_1 and τ_2 values and varying the amplitude of the gradient pulses (g). The results of this measurement are summarized in Fig. 4b. The value of τ_1 was set at 30 μs, 50 μs and 60 μs for $N@C_{60}$ in CS_2, $N@C_{60}$ in 1-chloronaphthalene, and trityl in water, respectively, while τ_2 was kept at 2.5 μs for all the experiments. The gradient amplitude was increased from 0 to 62 Tesla m^{-1}, 92 Tesla m^{-1} and 100 Tesla m^{-1} for $N@C_{60}$ in CS_2, $N@C_{60}$ in 1-chloronaphthalene, and trityl in water, respectively, in steps of ~7 Tesla m^{-1}. Here the results were corrected for the effect of the residual transient magnet fields that caused a non-optimal echo "signal reconstruction" (as explained in the discussion in section 5.1).

Table 1 summarizes the experimental data regarding unrestricted diffusion measurements and compares it to the theoretically-derived diffusion coefficient based on the Stokes–Einstein equation. It should be noted that the spherical shape of $N@C_{60}$ makes it a perfect molecule to fit the Stokes–Einstein theory, while the trityl is also fairly spherical but not as perfect as the C_{60}.

4.2 Restricted diffusion inside a matrix of glass spheres

Following the measurements of unrestricted diffusion, we examined the diffusion in porous media. Restricted diffusion was measured for the solution of trityl in water and for $N@C_{60}$ in CS_2 embedded in glass sub-microspheres, as described in Section 3.2. Trityl diffusion was measured for two different media, the first containing glass spheres with a diameter of 0.32 μm and the second containing spheres with a diameter of 0.51 μm. The restricted diffusion of $N@C_{60}$ in CS_2 was measured only for media of glass spheres with a diameter of 0.51 μm. All the experiments were carried out for τ_2 = 2.5 μs and the gradient amplitude was increased from 0 to 100 Tesla m^{-1} in equal steps of ~7 Tesla m^{-1}. The results for the two trityl samples were measured with τ_1 = 60 μs (*i.e.* Δ = 62.5 μs) and for $N@C_{60}$ it was measured for τ_1 of 30 μs (Δ = 32.5 μs). As before, every recorded echo subjected to the pulsed field gradients (denoted as s) was followed immediately by the recording of an echo signal without gradients (denoted as s_0). The ratio between the two signals (s/s_0) is free from relaxation effects and represents the diffusion-related signal decay (see eqn (2)), as well as the effect of the residual transient

Table 1 Summary of results of the PGSE ESR experiments for unrestricted diffusion

Sample	$N@C_{60}$ in 1-chloronaphthalene	$N@C_{60}$ in CS_2	Trityl in water
Solvent viscosity (mPa)[32,33]	3.02	0.35	1
Molecular radius (nm)[34,35]	0.51	0.51	0.75
Stokes–Einstein D value (m^2 s^{-1})	1.4×10^{-10}	1.2×10^{-9}	3.0×10^{-10}
Experimental D value from Fig. 4a (m^2 s^{-1})	$1.0 \times 10^{-10} \pm 0.1 \times 10^{-10}$	$1.2 \times 10^{-9} \pm 0.1 \times 10^{-9}$	$2.9\times 10^{-10} \pm 0.1 \times 10^{-10}$
Experimental D value from Fig. 4b (m^2 s^{-1})	$1.5 \times 10^{-10} \pm 0.1 \times 10^{-10}$	$1.6 \times 10^{-9} \pm 0.2 \times 10^{-9}$	$2.9\times 10^{-10} \pm 0.2 \times 10^{-10}$

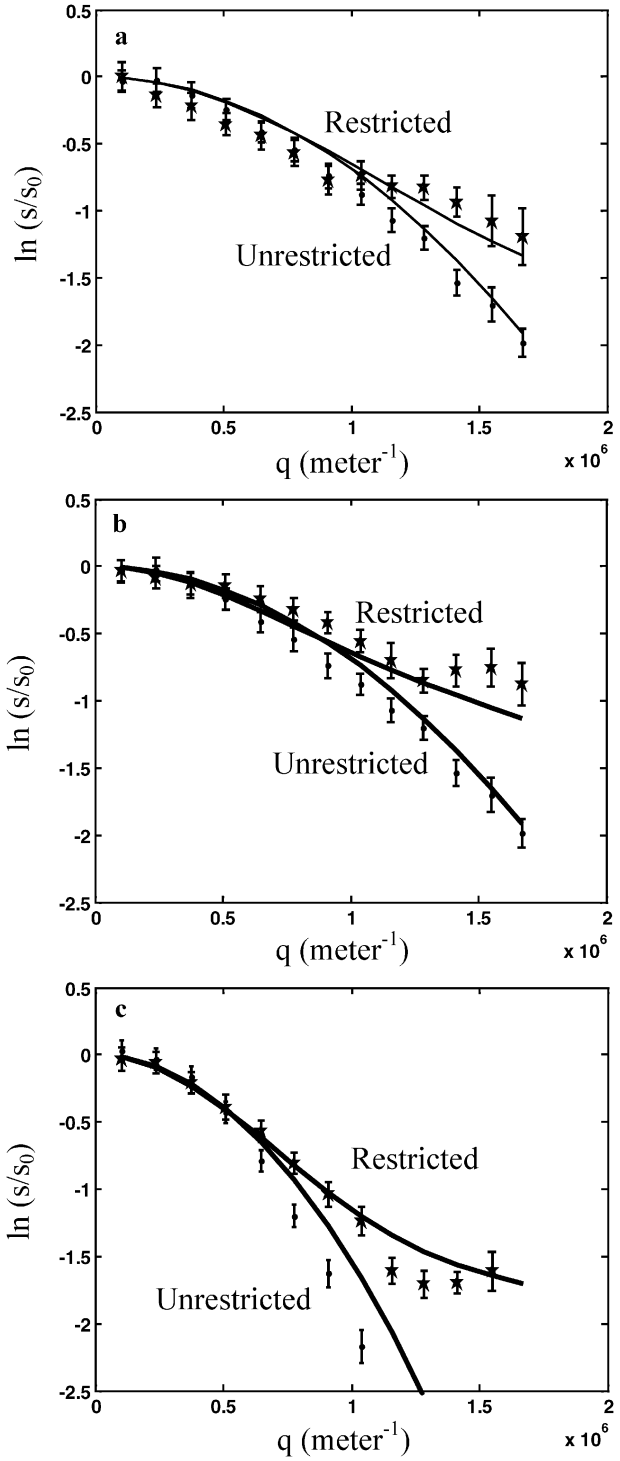

Fig. 5 Plots of $\ln(s/s_0)$ *vs.* $q = (2\pi)^{-1}\gamma \int_t^{t+\delta} g(t)\mathrm{d}t$ for solutions of trityl in water and N@C_{60} in CS_2 diffusing in unrestricted and restricted (porous) media. (a) Trityl solution embedded between a matrix composed of 0.32 μm glass microspheres (★) and a solution without the spheres (●). The theoretical curves, based on eqn (1) for the unrestricted case and eqn (2) for the restricted case, are shown in solid lines. (b) Same as (a) but for a trityl solution embedded in a matrix composed of 0.51 μm glass microsphere. The unrestricted results are of course the same as (a) and brought in this graph for comparison only. (c) N@C_{60} solution in CS_2 embedded between a matrix composed of 0.51 μm glass microspheres (★) and a solution without the spheres (●). The theoretical curves, based on eqn (1) for the unrestricted case and eqn (2) for the restricted case, are shown in solid lines.

magnetic fields of the gradient pulse at the time of the echo. The experimental data of $\ln(s/s_0)$ as a function of $q = (2\pi)^{-1}\gamma \int_t^{t+\delta} g(t)\mathrm{d}t$ for the restricted diffusion is shown in Fig. 5, together with the reference data for unrestricted diffusion in the homogenous solutions described above and the theoretical plots.

The theoretical plots for unrestricted diffusion are based on eqn (1) using the diffusion coefficient obtained from the Stokes–Einstein relation (see Table 1). The theoretical curves for restricted diffusion are based on eqn (2) with the following parameters (analogous to the NMR-PGSE work of diffusion inside a 16 μm spheres' matrix[5]): The effective diffusion coefficient, D_{eff}, was chosen to be the same as the theoretical diffusion coefficient for unrestricted diffusion provided in Table 1 (the theoretical Stokes–Einstein value is very similar to the measured values); the structure parameter b that represents the mean pore spacing was taken to be the glass spheres' diameter, the parameter a which represents the pores size was taken as $a = b/3$; and the standard deviation of b was taken as $\xi = b/6$.

5. Discussion

5.1 Unrestricted diffusion

As noted in Section 4.1, two types of measurements were employed to measure the unrestricted diffusion coefficient (*i.e.* with constant gradient and τ_2 while varying τ_1, and with constant τ_1 and τ_2 while varying the pulsed gradient amplitude). In principle, both methods should provide the same results, but in practice they are not equivalent, due to the effect of the residual transient magnetic fields. In the first method the transient effect is almost the same for all acquisition steps because the time between the second gradient pulse and the stimulated echo signal is kept constant. (We also use the reasonable assumption that the transient effect of the first gradient pulse on the echo signal is negligible.) This means that when τ_1 is increased, the corresponding additional normalized signal decay (s/s_0) should be only due to diffusion effects. The downside of this type of measurement is that in every acquisition step the diffusion is monitored over a different time interval. Thus, when one is interested in a diffusion process that occurs during a specific time frame (such as in the case of restricted diffusion), it is better to use the second type of measurement, with constant τ_1 and τ_2. However, in the second type of measurement one needs to carefully take into account the effect of the residual transient magnetic fields that grow as gradients become stronger. This means that when the gradient is increased, the corresponding additional normalized signal decay (s/s_0) is due to both diffusion effects and the increasing residual transient magnetic fields. To correct for this problem we use as reference the measurements of the N@C_{60} in 1-chloronaphthalene sample (as mentioned in Section 4.1), which provide us with the level of "signal reconstruction" at various combinations of gradient magnitudes and τ_1, t_2 intervals. The combined results from the two types of methods enable us to evaluate the accuracy of our measurements and the accuracy of the transient magnetic fields correction process.

It is clear from the plots in Fig. 4 and Table 1 that there is fairly good agreement between the theoretical estimations and the experimental results. Most of the measured D values are right at or very close (less than 5–10% deviation) to the expected calculated values. Still, although the quality of these graphs is far better than the ones presented in our previous work,[13] clearly more improvements can be made to obtain even better accuracy and more consistent results. The most probable reasons for the remaining inaccuracies are non-optimal corrections for the residual transient magnetic fields (as described above and in Section 4.1) during echo signal acquisition; also, some inaccuracies can be attributed to SNR and stability limitations. In principle, as explained above, the results of the first type of measurement (Fig. 4a) should be free of the transient magnetic fields effect and thus more accurate. The viscous sample of N@C_{60} in 1-chloronaphthalene is not much affected by diffusion and this leads to less accurate results for Fig. 4a—due to SNR and system stability limitations. The more accurate result for this sample in Fig. 4b is somewhat artificial, because, as noted in Section 4.1, this sample was used as a reference to evaluate and correct the effect of the residual transient magnetic fields for the other two samples in Fig. 4b. In this process we considered its theoretically-calculated diffusion coefficient. This leads, for this sample in Fig. 4b, to D value that is very close to the theoretical one because its experimental data were "self-corrected" with the same sample (but based on the results of two different sets of measurements).

Future possible improvements of the results can be made by higher SNR and smaller effect due to the residual transient magnetic fields. As for the SNR, it is clear that it should always be increased, which can be done by further improving the resonator geometry and working at higher magnetic fields (*e.g.* a probe at 35 GHz which is currently under construction). The residual transient magnetic fields can be further reduced by improving the electronic architecture of the gradient drivers and working with geometrically-similar samples. The latter issue is of importance because if the geometry of two samples differs considerably, they will experience different transient fields within the probe with different effects on their echo signals—thus making the correction process less accurate.

It can be concluded that with the present set-up unrestricted diffusion coefficients of paramagnetic species can be measured quite well for sub-millimolar concentrations for D in the order of $\sim 10^{-10}$–10^{-9} m^2 s^{-1} using $\tilde{q}$ values of up to 7×10^9 s m^{-2} (which is commonly known in the literature as "b value") and diffusion times of $\sim$10–100 μs (see also ref. 13).

5.2 Restricted diffusion

The experiments with restricted diffusion showed for the first time the possibility of applying PGSE ESR to characterize both morphological features and dynamical properties of motion in a simple but representative case of porous media. It is clear from Fig. 5 that a significant difference exists between the q-space spectrum of unrestricted and restricted diffusion, which also shows a reasonably good agreement between the theory and the experiments. The experimental data for the N@C_{60} in CS_2 sample show a lesser degree of agreement than those for the trityl sample. This is probably due to the lower SNR this sample exhibited (having lower spin concentration and faster diffusion decay), as well as to some uncorrected effects due to residual transient magnetic fields (these may vary from sample to sample, based on each sample's geometry—as mentioned above).

By comparison to simulated data, as shown in Fig. 5, the "q-space" signal can be readily used to provide good estimations regarding the size of the voids in porous media (a), the distance between pores (b), the standard deviation of b (ξ), and the effective diffusion coefficient from pore to pore (D_{eff}).[5] (The value of D_{eff} is approximately the same as D for unrestricted diffusion for these system. This is probably due to the fact that the pores are very large compared to the molecules' size and that motion from pore to pore does not cross any "membrane" or void with a different diffusion coefficient.) It should be noted that in the present set of experiments our gradient strength was not enough to observe "diffraction peaks" in the q-space signal.[5] This is because the present experimental capabilities are slightly short of meeting the two conditions described above for the observation of such diffraction peaks. The maximum value of q we could apply is $\sim 1.75 \times 10^6$ m^{-1}, which corresponds to a spatial resolution of $|q|^{-1} = 571$ nm. This means that even with the larger set of spheres we used, the minimal $|q|^{-1}$ value we obtained is still slightly larger than the spheres' diameter b (510 nm). An attempt to look at spheres with larger diameters is limited by the second condition requiring that $\Delta \approx b^2/2D_{eff}$, which in the case of spheres with a diameter larger than 510 nm implies a long diffusion time Δ that is longer than $\sim$110 μs for the relatively fast-diffusing N@C_{60} solution in CS_2 (and much more for the trityl solution). Such long diffusion times are currently not accessible with the present set-up due to SNR limitations (T_1 value). That is to say, the τ_1 values used for the experiments shown in Fig. 5 are the maximum we could get in the present system/sample combination while maintaining a reasonable SNR. Therefore, it is evident that in order to get a clear view of such "diffraction peaks" in future experiments (which is important for a better understanding of the morphology and the diffusion process), we should further increase our gradient values and aim at observing finer porous structures (with feature size in the range of $\sim$10–250 nm), at short diffusion times. This may be achieved using a smaller probe that is under construction and operates at 35 GHz with much smaller and more efficient gradient coils. Such probe will also have better SNR to allow for a longer diffusion time Δ.

5.3 Limitations of the current system and its future prospects

The experiments described above involved the use of paramagnetic species with exceptionally long relaxation times. While the use of such probes in their native form can be very useful for applications where diffusion properties in porous media are examined, many other applications of interest (see below) involve spin-labeled species. The vast majority of spin labeling techniques are based on nitroxide radicals that often have less favourable properties for PGSE ESR in terms of their relaxation times. For example, small nitroxides would typically have T_1 of $\sim$0.4–0.7 μs (and similar T_2 values), while

nitroxide-labeled lipids in fluid and gel-phase lipid bilayers have T_1 of $\sim$1–5 μs and 5–10 μs, respectively (with T_2 values that can be more than one order of magnitude shorter).[28] Clearly these values, especially the low T_2, would not enable our system in its present form to get any meaningful diffusion data. What is therefore needed in order to be able to try and employ PGSE ESR with at least some of the nitroxide-based species?

Based on our current experimental results for the 1 mM trityl solution, for example, one can see that a meaningful signal is obtained with τ_2 value that is $\sim\frac{1}{2}T_2$ and τ_1 values of up to almost $4T_1$. These values correspond to signal decay down to e^{-5} $\sim$0.7% of the maximum stimulated echo signal (see eqn (1)), even without any diffusion decay. Diffusion decay can reduce the signal by approximately two additional orders of magnitude, but still we get enough SNR in our experiments (with averaging), due to the high efficiency of the resonator we employ and to the large signal of the trityl radical. Going back to the nitroxide species, a possible PGSE ESR sequence would use τ_2 of $\sim$1.5–2T_2 (*i.e.* $\sim$200 ns—for the more favourable cases) and τ_1 value of up to 1–2T_1. This may allow observing diffusion in a time scale of up to a $\sim$10+ microseconds, with SNR similar to the one obtained for the trityl solution. The main methodological obstacle here would be the application of much shorter and more intense gradient pulses than those employed in the present work. Another challenge would be to excite most of the nitroxide spectrum with much shorter microwave pulses. Both challenges may be at closer reach with the next-generation 35 GHz probe (currently in its final assembly stages), which would also improve the overall SNR. This half-sized probe (compared to the present one) with gradient coils driven by a 1100 V source would generate gradients that are approximately 6 times larger in magnitude than the present system. This means that the effect of a 200 ns pulse (the gradient time integral) would be similar to that of the current 1.2 μs pulse. Clearly additional difficulties may be encountered, especially related to the decay time of such strong pulse (which can hopefully be reduced due to the lower inductance of the 35 GHz probe gradient coils). This near-future work may serve as an initial step towards broadening the scope of this methodology towards more common spin probes.

It can be concluded that this work showed how PGSE-ESR can complement the capabilities of PGSE NMR (and also of optical methods, see ref. 13) and observe diffusion typical to *aqueous environments* (commonly found in biology and materials science) in porous media in length- and time-scales that are inaccessible by other methods. In principle, such type of experiments can be performed using either soluble paramagnetic species or spin-labeled molecules. In such cases, the uniqueness of the ESR signal that can be attributed to a specific molecule can be used to differentiate between different types of motion of several species inside different compartments of complex or biological samples (while the NMR signal is in most cases attributed to the indistinguishable water signal). We envision that when the capabilities of PGSE are more fully developed it will be possible to address many important biological applications such as diffusion of molecules in and through porous cellular organelles (such as the centrosome), large-scale 3D intra-molecular dynamics of proteins or larger supra-molecular structures,[29] and characterizing different types of protein motion in non-homogenous cellular membranes.[17] Currently, however, the common method of labeling such biological molecules is with nitroxide spin labels, which are characterized (as noted above) by relaxation times (mainly T_2) that are too short for our current methodological capabilities. Still, a successful implementation of PGSE ESR in these scientific regimes may be achieved through further methodological developments, as described above, along with chemistry-related tasks, such as the possibility of developing new types of spin labels with longer relation times (*e.g.* based on the N@C_{60} or trityl species). Other applications that do not necessarily require labelling can come from the world of chemistry and materials science and include diffusion in porous catalytic pallets[30] and fuel cells.[31] Finally, PGSE may be combined with ESR micro imaging[27] to provide high-resolution spatially-resolved diffusion coefficients of spins in inhomogeneous samples.

Acknowledgements

This work was partially supported by grant no. 213/09 from the Israeli Science Foundation, grant no. 2005258 from the BSF foundation, grant no. 201665 from the European Research Council (ERC), and by the Russell Berrie Nanotechnology Institute at the Technion. The help and support of Arkady Gavrilov from the Technion Micro-Nano Fabrication Unit is greatly appreciated.

References and notes

1 *Transport in porous media*, D. Reidel Pub. Co., Dordrecht, Boston, 1986, p. v.
2 J. Bear and Y. Bachmat, *Introduction to modeling of transport phenomena in porous media*, Kluwer Academic Publishers, Dordrecht, Boston, 1991.
3 J. E. Tanner, *J. Chem. Phys.*, 1970, **52**, 2523–2526.
4 G. A. Barrall, L. Frydman and G. C. Chingas, *Science*, 1992, **255**, 714–717.
5 P. T. Callaghan, A. Coy, D. Macgowan, K. J. Packer and F. O. Zelaya, *Nature*, 1991, **351**, 467–469.
6 V. Kukla, J. Kornatowski, D. Demuth, I. Gimus, H. Pfeifer, L. V. C. Rees, S. Schunk, K. K. Unger and J. Karger, *Science*, 1996, **272**, 702–704.
7 C. Parravan, J. Baldesch and M. Boudart, *Science*, 1967, **155**, 1535–1536.
8 Y. Q. Song, S. G. Ryu and P. N. Sen, *Nature*, 2000, **406**, 178–181.
9 P. T. Callaghan, *Principles of nuclear magnetic resonance microscopy*, Clarendon Press; Oxford University Press, Oxford, England, 1991.
10 D. Candela, A. Ding and X. Y. Yang, *Phys. B*, 2000, **279**, 120–124.
11 H. Wassenius and P. T. Callaghan, *J. Magn. Reson.*, 2004, **169**, 250–256.
12 J. Mitchell and M. L. Johns, *Concepts Magn. Reson., Part A*, 2009, **34**, 1–15.
13 A. Blank, Y. Talmon, M. Shklyar, L. Shtirberg and W. Harneit, *Chem. Phys. Lett.*, 2008, **465**, 147–152.
14 C. Pappas, F. Mezei, A. Triolo and R. Zorn, *Phys. B*, 2005, **356**, 206–212.
15 N. B. Cole, C. L. Smith, N. Sciaky, M. Terasaki, M. Edidin and J. Lippincott Schwartz, *Science*, 1996, **273**, 797–801.
16 P. Schwille, U. Haupts, S. Maiti and W. W. Webb, *Biophys. J.*, 1999, **77**, 2251–2265.
17 T. Schmidt, G. J. Schutz, W. Baumgartner, H. J. Gruber and H. Schindler, *Proc. Natl. Acad. Sci. U. S. A.*, 1996, **93**, 2926–2929.

18 A. Schweiger and G. Jeschke, *Principles of pulse electron paramagnetic resonance*, Oxford University Press, Oxford, UK; New York, 2001.
19 P. T. Callaghan and J. Stepisnik, *Phys. Rev. Lett.*, 1995, **75**, 4532–4535.
20 G. Zheng, A. M. Torres and W. S. Price, *J. Magn. Reson.*, 2009, **198**, 271–274.
21 A. Feintuch, A. Grayevsky, N. Kaplan and E. Dormann, *Phys. Rev. Lett.*, 2004, **92**, 156803.
22 T. Tashma, G. Alexandrowicz, N. Kaplan, E. Dormann, A. Grayevsky and A. Gabay, *Synth. Met.*, 1999, **106**, 151–155.
23 T. Almeida Murphy, T. Pawlik, A. Weidinger, M. Hohne, R. Alcala and J. M. Spaeth, *Phys. Rev. Lett.*, 1996, **77**, 1075–1078.
24 W. Harneit, K. Huebener, B. Naydenov, S. Schaefer and M. Scheloske, *Phys. Status Solidi B*, 2007, **244**, 3879–3884.
25 P. Jakes, K. P. Dinse, C. Meyer, W. Harneit and A. Weidinger, *Phys. Chem. Chem. Phys.*, 2003, **5**, 4080–4083.
26 T. J. Reddy, T. Iwama, H. J. Halpern and V. H. Rawal, *J. Org. Chem.*, 2002, **67**, 4635–4639.
27 A. Blank, E. Suhovoy, R. Halevy, L. Shtirberg and W. Harneit, *Phys. Chem. Chem. Phys.*, 2009, **11**, 6689–6699.
28 L. J. Berliner, *Spin Labeling: The Next Millennium (Biological Magnetic Resonance), Vol. 14*, Plenum Press, New York, 1998.
29 G. C. K. Roberts, *Biochem. Soc. Trans.*, 2006, **34**, 971–974.
30 W. C. Cheng, N. P. Luthra and C. J. Pereira, *AIChE J.*, 1990, **36**, 559–564.
31 S. Srinivasan, *Fuel cells: from fundamentals to applications*, Springer, New York, 2006.
32 T. M. Aminabhavi and V. B. Patil, *J. Chem. Eng. Data*, 1998, **43**, 504–508.
33 T. Nakagawa, *J. Mol. Liq.*, 1995, **63**, 303–316.
34 T. Kato, K. Kikuchi and Y. Achiba, *J. Phys. Chem.*, 1993, **97**, 10251–10253.
35 R. Owenius, G. R. Eaton and S. S. Eaton, *J. Magn. Reson.*, 2005, **172**, 168–175.